



Gaia 0007–1605: An Old Triple System with an Inner Brown Dwarf–White Dwarf Binary and an Outer White Dwarf Companion

Alberto Rebassa-Mansergas^{1,2} , Siyi Xu (许偲艺)³ , Roberto Raddi¹ , Anna F. Pala⁴ , Enrique Solano^{5,6} ,
Santiago Torres^{1,2} , Francisco Jiménez-Esteban^{5,6} , and Patricia Cruz^{5,6}

¹ Departament de Física, Universitat Politècnica de Catalunya, c/ Esteve Terrades, 5, 08860 Castelldefels, Spain; alberto.rebassa@upc.edu

² Institut d'Estudis Espacials de Catalunya, Ed. Nexus-201, c/Gran Capità 2-4, 08034 Barcelona, Spain

³ Gemini Observatory/NSF's NOIRLab, 670 N. A'ohoku Place, Hilo, Hawaii, 96720, USA

⁴ European Space Agency, European Space Astronomy Centre, Camino Bajo del Castillo s/n, 28692 Villanueva de la Cañada, Madrid, Spain

⁵ Departamento de Astrofísica, Centro de Astrobiología (CSIC-INTA), ESAC Campus, Camino Bajo del Castillo s/n, E-28692 Villanueva de la Cañada, Madrid, Spain

⁶ Spanish Virtual Observatory, E-28692 Villanueva de la Cañada, Madrid, Spain

Received 2022 February 15; revised 2022 March 2; accepted 2022 March 3; published 2022 March 15

Abstract

We identify Gaia 0007–1605 A,C as the first inner brown dwarf–white dwarf binary of a hierarchical triple system in which the outer component is another white dwarf (Gaia 0007–1605 B). From optical/near-infrared spectroscopy obtained at the Very Large Telescope with the X-Shooter instrument and/or from Gaia photometry plus spectral energy distribution fitting, we determine the effective temperatures and masses of the two white dwarfs ($12,018 \pm 68$ K and $0.54 \pm 0.01 M_{\odot}$ for Gaia 0007–1605 A and 4445 ± 116 K and $0.56 \pm 0.05 M_{\odot}$ for Gaia 0007–1605 B) and the effective temperature of the brown dwarf (1850 ± 50 K; corresponding to spectral type $L3 \pm 1$). By analyzing the available TESS light curves of Gaia 0007–1605 A,C we detect a signal at 1.0446 ± 0.0015 days with an amplitude of 6.25 ppt, which we interpret as the orbital period modulated from irradiation effects of the white dwarf on the brown dwarf's surface. This drives us to speculate that the inner binary evolved through a common-envelope phase in the past. Using the outer white dwarf as a cosmochronometer and analyzing the kinematic properties of the system, we conclude that the triple system is about 10 Gyr old.

Unified Astronomy Thesaurus concepts: [White dwarf stars \(1799\)](#); [Trinary stars \(1714\)](#); [Brown dwarf stars \(185\)](#)

1. Introduction

Triple star systems are common, with fractions of $\simeq 10\%$ for F-G stars (Tokovinin et al. 2014) and increasing up to $\simeq 50\%$ for O-B stars (Sana et al. 2014). The majority of triple systems ($\simeq 70\%$ – 80%) are believed to interact during their lives (Toonen et al. 2020). Mass transfer episodes may take place from one star to another, in which case a common-envelope phase ensues if the process is dynamically unstable (Webbink 2008). Moreover—because the stellar components are subject to their individual evolutionary paths, thus changing their masses and radii if they have time to evolve out of the main sequence—three-body dynamics are expected to modify the systems, leading to tidal interactions, collisions, or mergers (Antonini et al. 2017). In this context, a clear example is the Von Zipel–Lidov–Kozai oscillations in hierarchical triples, with the outer component inducing eccentricity oscillations in the inner binary (Naoz 2016). Tides from the Galactic potential can also influence the orbits of the stars in triple systems (Grishin & Perets 2021). These mechanisms may lead to exotic outcomes, such as blue stragglers (Perets & Fabrycky 2009), black holes (Antonini et al. 2017), neutron star mergers (Liu & Lai 2018), Type Ia supernovae (Katz & Dong 2012), or gamma-ray bursts (Thompson 2011).

Given the variety of possible evolutionary scenarios, triple systems come in different flavors: main-sequence triples (Kervella et al. 2017), main-sequence/brown dwarf triples

(Faherty et al. 2011), brown dwarf triples (Triaid et al. 2020), giant-star/brown dwarf triples (Lillo-Box et al. 2021), main-sequence/white dwarf triples (Toonen et al. 2017), main-sequence/black hole triples (Rivinius et al. 2020), white dwarf triples (Perpinyà-Vallès et al. 2019), white dwarf/neutron star triples (Ransom et al. 2014), etc. Hence, observational studies of triple systems are not only important for constraining our understanding of multiple stellar evolutions but also to elucidate the origin of such exotic objects.

In this work, we identify the first trinary star formed by two white dwarfs and a brown dwarf. The structure of the system is hierarchical, with an inner white dwarf–brown dwarf binary (hereafter Gaia 0007–1605 A,C) and a wider white dwarf companion (hereafter Gaia 0007–1605 B). Using the outer white dwarf as a cosmochronometer, we find this unique system to be nearly as old as the age of the Galactic disk, thus implying the brown dwarf to be one of the oldest known of its kind.

2. Identification of Gaia 0007–1605

Gaia 0007–1605 A,C (ID 2416481783371550976), also known as EGGR 509, was identified as an infrared-excess white dwarf candidate by Rebassa-Mansergas et al. (2019), who analyzed the spectral energy distributions (SED) of 3733 Gaia white dwarfs within 100 pc with reliable infrared photometry and $G_{BP} - G_{RP} < 0.8$ mag. We obtained a spectrum (430 s exposure) for this object with the Very Large Telescope at Cerro Paranal (Chile) equipped with the X-Shooter instrument and the $1''$ slits on the night of 2020December 3, which revealed the infrared excess to arise

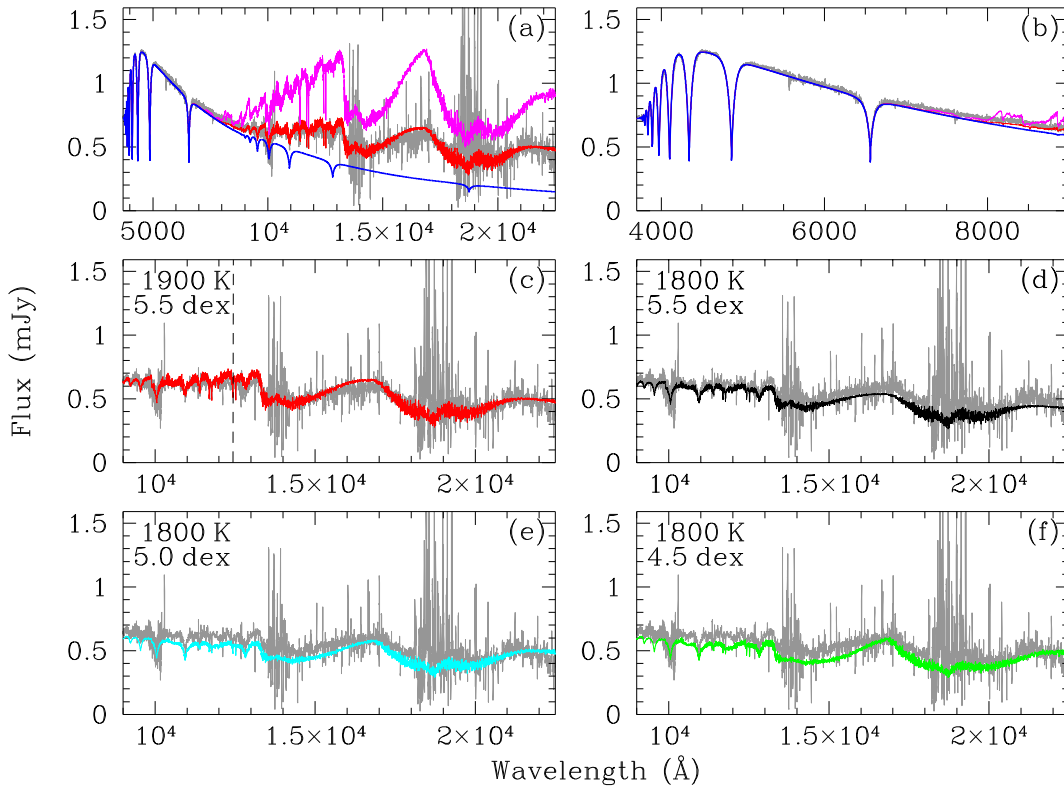


Figure 1. Panel (a): the observed X-Shooter spectrum of Gaia 0007–1605 A,C (gray), the best-fit white dwarf model (blue) and its combination with a 2300 K and 5.0 dex CIFIST model (magenta; corresponding to a star of spectral type M9.5) and a 1900 K and 5.5 dex CIFIST model, i.e., the best fit to the observed spectrum. An M9.5 companion can clearly be ruled out, which confirms the near-infrared excess to arise from a brown dwarf. The structure at $\simeq 14,000$ Å and $\simeq 19,000$ Å is related to the residuals of the telluric correction. Panel (b): the same but for the optical range of the spectrum, where the white dwarf dominates the SED. Panel (c): the combined best fit to the near-infrared range of the spectrum. The effective temperature and surface gravity of the brown dwarf are indicated in the top-left corner and the dashed vertical line indicates the K_1 12 432.27/12 522.14 Å absorption doublet from which we measure the radial velocity. Panels (d), (e), and (f): for comparison, we show the second-best (d), third-best (e), and fourth-best (f) CIFIST models superimposed on the observed near-infrared spectrum. The effective temperatures and surface gravities are also indicated.

Table 1
Gaia EDR3 Parameters (Riello et al. 2021) for the Inner Unresolved Binary (Gaia 0007–1605 A,C) and the Outer White Dwarf (Gaia 0007–1605 B)

Object	R.A.	Decl.	G	G_{BP}	G_{GRP}	$pm_{R.A.}$	$pm_{Decl.}$	parallax
(1)	(deg)	(deg)	(mag)	(mag)	(mag)	(mas/yr)	(mas/yr)	(mas)
(1)	(2)	(3)	(4)	(5)	(6)	(7)	(8)	(9)
Gaia 0007–1605 A,C	1.895921	−16.09240	16.152 ± 0.003	16.162 ± 0.004	16.157 ± 0.008	179.23 ± 0.05	$−64.40 \pm 0.04$	12.34 ± 0.04
Gaia 0007–1605 B	1.893281	−16.08726	19.942 ± 0.005	20.59 ± 0.08	19.24 ± 0.05	176.36 ± 0.61	$−64.11 \pm 0.41$	12.53 ± 0.55

due to the presence of a brown dwarf companion⁷ (see Figure 1).

The measured Gaia parallax of Gaia 0007–1605 A,C is 12.34 ± 0.04 mas (Table 1) and the inverse parallax yields a distance of 81.1 ± 0.1 pc. El-Badry et al. (2021) and Rebassa-Mansergas et al. (2021) report this object as a common proper-motion pair member with a second white dwarf (ID 2416481779075909376) at the same distance and proper motions (Table 1). The projected separation between Gaia 0007–1605 A,C and the outer white dwarf Gaia 0007–1605 B is 1673.11 au (El-Badry et al. 2021), and the radial separation is 1.2 pc (Torres et al. 2022).

3. Stellar Parameters of the Three Components

We derived three independent values of effective temperature and surface gravity for the inner white dwarf Gaia 0007–1605 A from (1) the available Gaia EDR3 G_{abs} and $G_{BP} - G_{GRP}$ colors following the method described in Rebassa-Mansergas et al. (2021);⁸ $T_{eff} = 11,814 \pm 142$ K and $\log g = 7.86 \pm 0.02$ dex; (2) fitting the entire SED using VOSA (Virtual Observatory SED Analyser)⁹ following Jiménez-Esteban et al. (2018): $T_{eff} = 12,000 \pm 125$ K and $\log g = 7.84 \pm 0.03$ dex; the passbands used in the fit were GALEX NUV/FUV, APASS BgVi, Pan-STARRS *grizy*, Gaia

⁷ The spectra were reduced/calibrated using the X-Shooter pipeline version 2.11.5. Telluric removal was performed using the Molecfit software.

⁸ Note that the brown dwarf in the inner binary is completely outshined in the optical by the flux of the white dwarf. Only for wavelengths larger than 8000 Å is the average excess flux contribution from the brown dwarf $\simeq 5\%$. Therefore, the reported Gaia magnitudes can be safely considered as those arising from the white dwarf only.

⁹ The VOSA documentation can be accessed via <http://svo2.cab.inta-csic.es/theory/vosa/help/star/intro>.

Table 2
Stellar Parameters and Ages for the Triple System Studied in This Work

Object	Type	T_{eff} (K)	$\log g$ (dex)	mass (M_{\odot})	t_{cool} (Gyr)	Total Age (Gyr)	P_{orb} (days)	Method
(1)	(2)	(3)	(4)	(5)	(6)	(7)	(8)	(9)
Gaia 0007–1605 A	DA	12018 ± 68	7.87 ± 0.02	0.54 ± 0.01	0.360 ± 0.002	$\approx 10^{\text{a}}$	1.0446 ± 0.0015	Phot./Spect.
Gaia 0007–1605 C	L3	1850 ± 50	...	0.07^{a}	...	$\approx 10^{\text{a}}$	1.0446 ± 0.0015	Spect.
Gaia 0007–1605 B	pure-H DC ^a	4445 ± 116	7.96 ± 0.05	0.56 ± 0.05	8.2 ± 0.2	$\approx 10^{\text{a}}$...	Phot.

Note. The method used to derive the effective temperatures is also indicated. The values and parameters indicated by an

^a Assumptions and require confirmation.

EDR3 $G/G_{\text{BP}}/G_{\text{RP}}$, DENIS II, 2MASS JHK , and WISE w1w2; (3) fitting the optical X-Shooter spectrum with the updated grid of white dwarf model atmosphere spectra of Koester (2010), taking into account the 3D corrections by Tremblay et al. (2013): $T_{\text{eff}} = 12,131 \pm 100$ K and $\log g = 7.97 \pm 0.04$ dex; the best-fit white dwarf model is illustrated in Figure 1. The weighted mean yields $T_{\text{eff}} = 12,018 \pm 68$ K and $\log g = 7.87 \pm 0.02$ dex, which are our adopted parameters for this white dwarf (Table 2). For the outer white dwarf Gaia 0007–1605 C, there is no available sets of parameters from the Gaia G_{abs} and $G_{\text{BP}} - G_{\text{RP}}$ colors ($T_{\text{eff}} = 4121 \pm 304$ K and $\log g = 7.8 \pm 0.2$ dex) and VOSA ($T_{\text{eff}} = 4500 \pm 125$ K and $\log g = 8.0 \pm 0.1$ dex); the passbands used in the fit were Pan-STARRS *grizy*, Gaia EDR3 $G/G_{\text{BP}}/G_{\text{RP}}$, and WISE w1). Hence, our adopted values are $T_{\text{eff}} = 4445 \pm 116$ K and $\log g = 7.96 \pm 0.05$ dex for the outer white dwarf (Table 2). We then interpolated the adopted effective temperatures and surface gravities of the white dwarfs in the cooling sequences of the La Plata group (Althaus et al. 2015; Camisassa et al. 2016, 2019) to obtain their masses (Table 2).

For the above calculations, we assumed the two white dwarfs to have hydrogen-rich atmospheres. This is confirmed for the inner white dwarf (Figure 1) but it has not been tested for Gaia 0007–1605 C. For this object, Gentile Fusillo et al. (2021) derives 4500 ± 400 K (assuming either a hydrogen-rich or helium-rich atmosphere), in agreement with our value. At such low effective temperature, a spectrum would be featureless (DC type), hence giving no indications about the atmospheric composition of this white dwarf.

In order to derive the brown dwarf parameters, we performed a composite spectral fit. We created a set of composite models that combine the white dwarf best-fit model with a grid of BT-Settl (CIFIST; Allard et al. 2013, only at solar metallicity¹⁰) low-mass and brown dwarf model spectra and obtained a χ^2 value between the observed X-Shooter spectrum and each combined model. The CIFIST grid contained 42 spectra with effective temperatures in the range 1300–2600 K in steps of 100 K and surface gravities of 4.5–5.5 dex in steps of 0.5 dex. All models were scaled to the distance of 81.1 pc by assuming a radius from an effective temperature–radius relation for low-mass stars and brown dwarfs (Pecaut & Mamajek 2013; Baraffe et al. 2015) and an effective temperature–radius relation for white dwarfs from the La Plata tracks. The CIFIST model associated with the lowest χ^2 (χ_{min}^2) was that of an effective temperature of 1900 K and a surface gravity of 5.5

dex (Figure 1). Considering all models at a distance of less than 1σ from χ_{min}^2 as valid solutions resulted in temperatures in the range 1800–1900 K with all possible surface gravities (4.5, 5.0, and 5.5 dex; Figure 1). Therefore, we cannot constrain the surface gravity of the brown dwarf but we can estimate its temperature to be 1850 ± 50 K. This corresponds to a spectral type of $L3 \pm 1$ (Nakajima et al. 2004).

4. Observational Clues on the Past Evolution of the Inner Binary

Gaia 0007–1605 A,C is unresolved by Gaia, which probably implies it evolved through a common-envelope phase. In order to test this hypothesis, we searched for available time-series photometry from the Mikulski Archive for Space Telescopes, finding that this object was observed by the Transit Exoplanet Survey Satellite (TESS; Ricker et al. 2015) in Sector 29 as TIC 289593425, between 2020 August 26 and September 21. We analyzed the 20 s and 2 and 10 minute cadence data using standard tools of the *lightcurve* software, finding a peak at 1.0446 ± 0.0015 days in the Lomb–Scargle periodogram of the 10 minute cadence light-curve (see Figure 2, top panel). This peak corresponds to a signal amplitude of 6.25 ppt that is just above the 0.1% false-alarm-probability limit that we computed as in Hermes et al. (2017), meaning that the detection has a probability higher than 99.9% of not being caused by noise. In Figure 2 (middle and bottom panels), we show the folded light curve for this period. The light curve is clearly noisy; however, by binning it at every 30 minutes we are able to highlight the periodic variability detected by TESS. We interpret the signal at 1.0446 day period as the irradiation of the white dwarf on the brown dwarf’s surface that becomes visible to us every orbit.

The ratio between the brown dwarf’s flux (F_{BD}) and the irradiated flux from the white dwarf on the brown dwarf’s surface (F_{irr}) can be expressed as (Rebassa-Mansergas et al. 2013)

$$\frac{F_{\text{BD}}}{F_{\text{irr}}} = \left(\frac{T_{\text{eff,BD}}}{T_{\text{eff,WD}}} \right)^4 \times \left(\frac{a}{R_{\text{WD}}} \right)^2, \quad (1)$$

where $T_{\text{eff,BD}}$ and $T_{\text{eff,WD}}$ are the brown dwarf and white dwarf effective temperatures, R_{WD} is the white dwarf radius, and a is the orbital separation. All are known parameters (Section 3; note that the white dwarf radius can be obtained from the surface gravity and mass reported in Table 2) except a , which we derived from Kepler’s third law assuming 1.0446 days as the orbital period of the binary as well as via adopting a white dwarf and a brown dwarf mass. The mass of the white dwarf is known, but the brown dwarf’s mass is not. However, following

¹⁰ We also used low-metallicity NextGen models to evaluate whether the brown dwarf could be an ultracool subdwarf star but found no good fits in any of these cases.

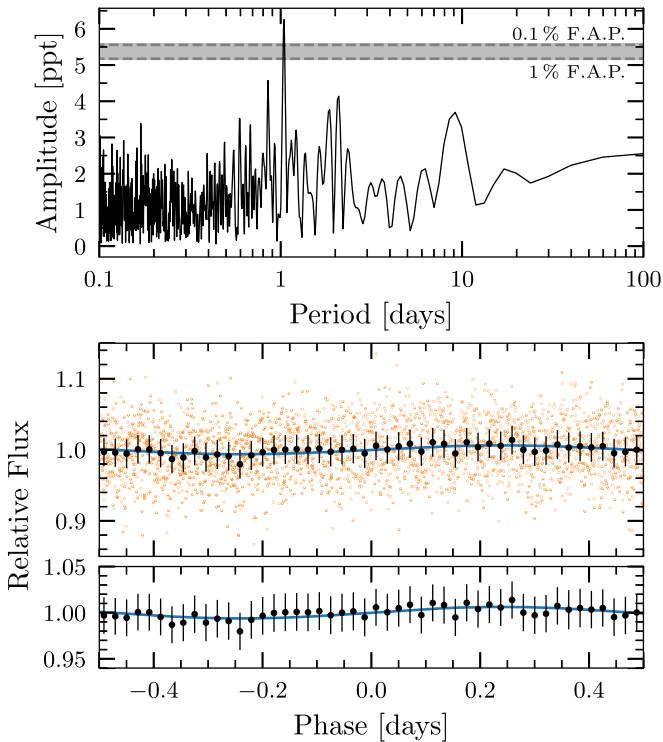


Figure 2. Top panel: Lomb–Scargle periodogram of the TESS light curve. The strongest signal at 1.0446 ± 0.0015 days exceeds the 1 and 0.1% false-alarm-probability (F. A. P.) thresholds. Middle panel: folded light curve, obtained from the 1.0446 day period. The black symbols are the binned light curve at 30 minute intervals, and the error bars represent the 1σ scatter in each bin. The blue sinusoidal curve corresponds to the detected periodic signal. Bottom panel: zoomed panel on the binned light curve.

the spectral type–mass relation of Pecaut & Mamajek (2013),¹¹ we estimated the mass to be $0.07 M_{\odot}$. Given that the white dwarf’s mass is considerably higher than the brown dwarf’s mass, the orbital separation does not heavily depend on this assumption. In fact, using masses between 0.05 and $0.1 M_{\odot}$ yielded practically identical orbital separations. The top and bottom panels of Figure 3 show the flux ratio and orbital separation as a function of the orbital period, respectively, which correspond to $F_{\text{BD}}/F_{\text{irr}} = 40$ and $a = 3.65 R_{\odot}$ for a period of 1.0446 days.

Based on the above calculations, the fraction of irradiated flux from the white dwarf on the brown dwarf’s surface is $\simeq 2.5\%$ of the total flux. This percentage should be lower if one considers the $6000\text{--}10000 \text{ \AA}$ range sampled by the TESS bandpass filter because the white dwarf’s flux peaks in the ultraviolet. This is in agreement with the amplitude modulation of $\simeq 0.5\%$ in the folded light curve (middle and bottom panels of Figure 2).

For completeness, we also derived the radial velocity of the brown dwarf by fitting the K_1 absorption doublet at $12\,432.27/12\,522.14 \text{ \AA}$ from the X-Shooter spectrum with a double-Gaussian profile of fixed separation. To that end we used the MOLLY software, resulting in $42 \pm 11 \text{ km s}^{-1}$, which unfortunately did not provide much information because we do not know the orbital inclination of the inner binary nor the orbital phase at which the spectrum was taken. For the white dwarf,

¹¹ See also http://www.pas.rochester.edu/~emamajek/EEM_dwarf_UBVIJHK_colors_Teff.dat.

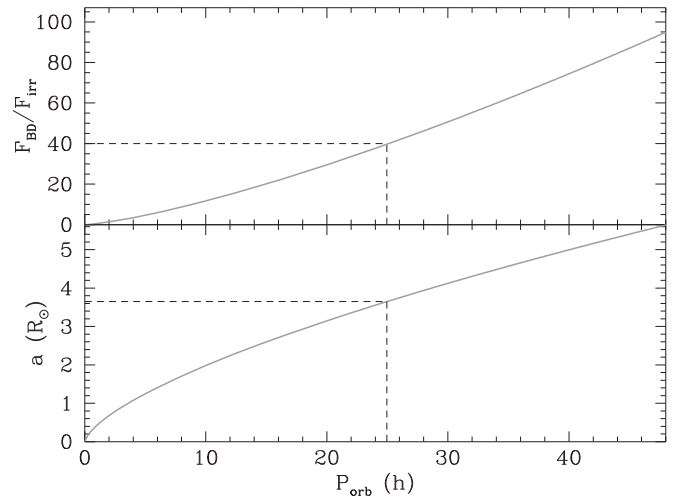


Figure 3. Top panel: the ratio between the brown dwarf’s flux (F_{BD}) and the irradiated flux from the white dwarf on the brown dwarf’s surface (F_{irr}) as a function of orbital period. Bottom panel: the orbital separation as a function of orbital period. The dashed black lines represent the values for 1.0446 days, which is assumed to be the orbital period of Gaia 0007–1605 A,C.

radial velocities of 13.1 ± 2.5 and $15.5 \pm 1.3 \text{ km s}^{-1}$ were measured by the SPY high-resolution survey (Napiwotzki et al. 2020). This implies a minimum orbital inclination of the inner binary toward the line of sight of $\gtrsim 45^\circ$.

We conclude that Gaia 0007–1605 A,C likely evolved through a common-envelope phase and has now an orbital period of 1.0446 ± 0.0015 days.

5. The Age of the System

Given that two white dwarfs are members of the triple system studied in this work, we can independently derive two total ages by summing up the white dwarf cooling ages to the main-sequence progenitor lifetimes. To that end, we follow the procedure described in Rebassa-Mansergas et al. (2021), which considers the La Plata evolutionary tracks taking into account the full evolutionary path of the white dwarf from the zero-age main sequence. In these sequences, the mass of the hydrogen envelope is not fixed but obtained from evolutionary calculations.

The white dwarf in the inner binary has likely evolved through a common-envelope phase. As consequence, we can only derive its cooling age (Table 2) because applying an initial-to-final-mass relation to derive the progenitor lifetime would not be adequate. The outer white dwarf is located 1.2 pc away from the inner binary (Section 2). Hence, it is expected that it evolved in isolation. Taking into account the uncertainties in the derived effective temperature and surface gravity, we obtained a cooling age of $8.2 \pm 0.2 \text{ Gyr}$. Therefore, 8 Gyr is the 1σ lower limit to the age of the system because we need to add the progenitor lifetime (which we cannot obtain because the initial-to-final-mass relation is not well defined for white dwarf masses under $\lesssim 0.55 M_{\odot}$).

The random forest analysis of the 100 pc white dwarf Gaia population by Torres et al. (2019) indicates that the white dwarf in the inner binary is a thin-disk candidate, whereas the outer white dwarf is a thick-disk candidate. This is mainly due to the different temperatures (hence cooling ages) of the white dwarfs (Table 2). Additionally, we performed Galactic orbit integration for the inner binary and the distant companion by adopting

either a null value or the brown dwarf’s radial velocity (Section 4) and using the five Gaia astrometric parameters and correlations, as we followed the methods outlined by Raddi et al. (2022). In both cases, the orbital eccentricity and the Z component of the angular momentum of the two white dwarfs are in the region of $e = 0.16$ and $L_z = 1700 \text{ kpc km s}^{-1}$, which is at the separation between thin- and thick-disk orbits. This supports the idea of the triple system being rather old, as expected from the cooling age we obtained for the outer white dwarf. If we set the total age limit to $\simeq 10 \text{ Gyr}$, which is the mean age of the thick disk (Sharma et al. 2019), the stellar parameters for the outer white dwarf that are consistent with this value within $\pm 0.5 \text{ Gyr}$ errors are the following: $\simeq 4400 \text{ K}$ for the effective temperature, $\simeq 8.0 \text{ dex}$ of surface gravity, and $\simeq 0.6 M_\odot$ of mass. These values are in agreement with the estimates of $4500 \pm 400 \text{ K}$, $8.0 \pm 0.3 \text{ dex}$, and $0.6 \pm 0.20 M_\odot$ obtained by Gentile Fusillo et al. (2021) for this white dwarf assuming either hydrogen- or helium-rich atmospheres. We thus conclude that the age of the triple system studied in this work is around 10 Gyr .

6. Conclusions

We have identified and analyzed a remarkable hierarchical triple system formed by an inner brown dwarf–white dwarf binary and an outer white dwarf companion, the first of its kind. The most likely scenario is that Gaia 0007–1605 A and C were relatively close binaries during the main-sequence stage of Gaia 0007–1605 A and evolved through a common-envelope phase, while Gaia 0007–1605 B evolved like a single star. Alternatively, it is possible that Gaia 0007–1605 C was scattered to the current position after Gaia 0007–1605 A became a white dwarf, through different dynamical interactions (e.g., O’Connor et al. 2021). Additional modeling is needed to understand the evolutionary history of this interesting system.

Using the outer white dwarf as a cosmochronometer and analyzing the kinematic properties of the system, we find that the trinary star is very old and has an age of $\simeq 10 \text{ Gyr}$. Being nearly as old as the disk of the galaxy, the brown dwarf Gaia 0007–1605 C is not expected to be magnetically active nor rapidly rotating unless it is tidally locked by the white dwarf. Therefore, it could potentially be used as a benchmark for testing theoretical models of brown dwarfs. In particular, future observations with the James Webb Space Telescope can help in improving the measurements of the stellar parameters of this object.

A.R.M. acknowledges support from Grant RYC-2016–20254 funded by MCIN/AEI/10.13039/501100011033 and by ESF Investing in your future. S.X. is supported by the international Gemini Observatory, a program of NSF’s NOIRLab, which is managed by the Association of Universities for Research in Astronomy (AURA) under a cooperative agreement with the National Science Foundation, on behalf of the Gemini partnership of Argentina, Brazil, Canada, Chile, the Republic of Korea, and the United States of America. R.R. has received funding from the postdoctoral fellowship program Beatrú de Pinós, funded by the Secretary of Universities and Research (Government of Catalonia) and by the Horizon 2020 program of research and innovation of the European Union under the Maria Skłodowska-Curie grant agreement No. 801370. S.T. and A.R.M. acknowledge support from the MINECO under the PID2020-117252GB-I00 grant. F.









J.E. acknowledges financial support from the Spanish MINECO/FEDER through the grant MDM-2017–0737 at Centro de Astrobiología (CSIC-INTA), Unidad de Excelencia María de Maeztu. P.C. acknowledges financial support from the Government of Comunidad Autónoma de Madrid (Spain), via postdoctoral grant Atracción de Talento Investigador 2019-T2/TIC-14760. This research has made use of the Spanish Virtual Observatory (<http://svo.cab.inta-csic.es>) supported by Ministerio de Ciencia e Innovación through grant PID2020-112949GB-I00. This work has made use of data from the European Space Agency (ESA) mission Gaia (<https://www.cosmos.esa.int/gaia>), processed by the Gaia Data Processing and Analysis Consortium (DPAC, <https://www.cosmos.esa.int/web/gaia/dpac/consortium>). Funding for the DPAC has been provided by national institutions, in particular the institutions participating in the Gaia Multilateral Agreement.

Based on observations collected at the European Organisation for Astronomical Research in the Southern Hemisphere under ESO program(s) 106.213V.001 and 0106.D-0386(A).

Facility: VLT (X-SHOOTER).

Software: Molecfit (Kausch et al. 2015), Reflex (Freudling et al. 2013), astroquery (Ginsburg et al. 2019), galpy v1.6 (Bovy 2015), lightkurve (Lightkurve Collaboration et al. 2018), VOSA (Bayo et al. 2008), MOLLY (developed by Tom Marsh and available at <http://deneb.astro.warwick.ac.uk/phsaap/software>).

ORCID iDs

Alberto Rebassa-Mansergas  <https://orcid.org/0000-0002-6153-7173>
 Siyi Xu (许偲艺)  <https://orcid.org/0000-0002-8808-4282>
 Roberto Raddi  <https://orcid.org/0000-0002-9090-9191>
 Anna F. Pala  <https://orcid.org/0000-0001-7069-7403>
 Enrique Solano  <https://orcid.org/0000-0003-1885-5130>
 Santiago Torres  <https://orcid.org/0000-0001-5777-5251>
 Francisco Jiménez-Esteban  <https://orcid.org/0000-0002-6985-9476>
 Patricia Cruz  <https://orcid.org/0000-0003-1793-200X>

References

- Allard, F., Homeier, D., Freytag, B., Schaffenberger, W., & Rajpurohit, A. S. 2013, *MSAIS*, **24**, 128
 Althaus, L. G., Camisassa, M. E., Miller Bertolami, M. M., Córscico, A. H., & García-Berro, E. 2015, *A&A*, **576**, A9
 Antonini, F., Toonen, S., & Hamers, A. S. 2017, *ApJ*, **841**, 77
 Baraffe, I., Homeier, D., Allard, F., & Chabrier, G. 2015, *A&A*, **577**, A42
 Bayo, A., Rodrigo, C., Barrado Y Navascués, D., et al. 2008, *A&A*, **492**, 277
 Bovy, J. 2015, *ApJS*, **216**, 29
 Camisassa, M. E., Althaus, L. G., Córscico, A. H., et al. 2016, *ApJ*, **823**, 158
 Camisassa, M. E., Althaus, L. G., Córscico, A. H., et al. 2019, *A&A*, **625**, A87
 El-Badry, K., Rix, H.-W., & Heintz, T. M. 2021, *MNRAS*, **506**, 2269
 Faherty, J. K., Burgasser, A. J., Bochanski, J. J., et al. 2011, *AJ*, **141**, 71
 Freudling, W., Romaniello, M., Bramich, D. M., et al. 2013, *A&A*, **559**, A96
 Gentile Fusillo, N. P., Tremblay, P. E., Cukanovaite, E., et al. 2021, *MNRAS*, **508**, 3877
 Ginsburg, A., Sipőcz, B. M., Brasseur, C. E., et al. 2019, *AJ*, **157**, 98
 Grishin, E., & Perets, H. B. 2021, arXiv:2112.11475
 Hermes, J. J., Gänsicke, B. T., Kawaler, S. D., et al. 2017, *ApJS*, **232**, 23
 Jiménez-Esteban, F. M., Torres, S., Rebassa-Mansergas, A., et al. 2018, *MNRAS*, **480**, 4505
 Katz, B., & Dong, S. 2012, arXiv:1211.4584
 Kausch, W., Noll, S., Smette, A., et al. 2015, *A&A*, **576**, A78
 Kervella, P., Thévenin, F., & Lovis, C. 2017, *A&A*, **598**, L7
 Koester, D. 2010, *MmSAI*, **81**, 921

- Lightkurve Collaboration, Cardoso, J. V. D. M., Hedges, C., et al. 2018, Lightkurve: Kepler and TESS time series analysis in Python, *Astrophysics Source Code Library*, ascl:1812.013
- Lillo-Box, J., Ribas, Á, Montesinos, B., et al. 2021, *A&A*, **653**, A40
- Liu, B., & Lai, D. 2018, *ApJ*, **863**, 68
- Nakajima, T., Tsuji, T., & Yanagisawa, K. 2004, *ApJ*, **607**, 499
- Naoz, S. 2016, *ARA&A*, **54**, 441
- Napiwotzki, R., Karl, C. A., Lisker, T., et al. 2020, *A&A*, **638**, A131
- O'Connor, C. E., Liu, B., & Lai, D. 2021, *MNRAS*, **501**, 507
- Pecaut, M. J., & Mamajek, E. E. 2013, *ApJS*, **208**, 9
- Perets, H. B., & Fabrycky, D. C. 2009, *ApJ*, **697**, 1048
- Perpinyà-Vallès, M., Rebassa-Mansergas, A., Gänsicke, B. T., et al. 2019, *MNRAS*, **483**, 901
- Raddi, R., Torres, S., Rebassa-Mansergas, A., et al. 2022, *A&A*, **658**, A22
- Ransom, S. M., Stairs, I. H., Archibald, A. M., et al. 2014, *Natur*, **505**, 520
- Rebassa-Mansergas, A., Schreiber, M. R., & Gänsicke, B. T. 2013, *MNRAS*, **429**, 3570
- Rebassa-Mansergas, A., Solano, E., Xu, S., et al. 2019, *MNRAS*, **489**, 3990
- Rebassa-Mansergas, A., Maldonado, J., Raddi, R., et al. 2021, *MNRAS*, **505**, 3165
- Ricker, G. R., Winn, J. N., Vanderspek, R., et al. 2015, *JATIS*, **1**, 014003
- Riello, M., De Angeli, F., Evans, D. W., et al. 2021, *A&A*, **649**, A3
- Rivinius, T., Baade, D., Hadrava, P., Heida, M., & Klement, R. 2020, *A&A*, **637**, L3
- Sana, H., Le Bouquin, J. B., Lacour, S., et al. 2014, *ApJS*, **215**, 15
- Sharma, S., Stello, D., Bland-Hawthorn, J., et al. 2019, *MNRAS*, **490**, 5335
- Thompson, T. A. 2011, *ApJ*, **741**, 82
- Tokovinin, A., Mason, B. D., & Hartkopf, W. I. 2014, *AJ*, **147**, 123
- Toonen, S., Hollands, M., Gänsicke, B. T., & Boekholt, T. 2017, *A&A*, **602**, A16
- Toonen, S., Portegies Zwart, S., Hamers, A. S., & Bandopadhyay, D. 2020, *A&A*, **640**, A16
- Torres, S., Canals, P., Jiménez-Esteban, F. M., Rebassa-Mansergas, A., & Solano, E. 2022, arXiv:2202.04199
- Torres, S., Cantero, C., Rebassa-Mansergas, A., et al. 2019, *MNRAS*, **485**, 5573
- Tremblay, P. E., Ludwig, H. G., Steffen, M., & Freytag, B. 2013, *A&A*, **559**, A104
- Triaud, A. H. M. J., Burgasser, A. J., Burdanov, A., et al. 2020, *NatAs*, **4**, 650
- Webbink, R. F. 2008, in *Astrophysics and Space Science Library*, ed. E. F. Milone, D. A. Leahy, & D. W. Hobill, 352 (Berlin: Springer), 233